

Comparison of the performance of round and rectangular wire in small solenoids for high-field NMR[†]

Yu Li,¹ Andrew G. Webb,² Saikat Saha,³ William W. Brey,³ Cherian Zachariah¹ and Arthur S. Edison^{1,3*}

¹ Department of Biochemistry and Molecular Biology and McKnight Brain Institute, University of Florida, USA

² Department of Bioengineering, 206 Hallowell Building, Penn State University, PA, USA

³ National High Magnetic Field Lab, Tallahassee, FL, USA

Received 1 September 2005; Revised 21 November 2005; Accepted 1 December 2005

This paper considers the effects of conductor geometry on the performance of small solenoidal coils for high-field NMR. First, a simple analytical model is presented for investigating the effects of conductor geometry on the current distribution in such coils. The model was used to derive optimum parameters for coils constructed from wire with either rectangular or circular cross-sections as a function of the length-to-diameter ratio. Second, a commercial software package utilizing full three-dimensional finite-element solutions to Maxwell's equations was used to confirm the basic findings of the simple analytical model, and also to compare simulated S/N estimations with experimental NMR spectra acquired with 2.5 mm and 1.0 mm-diameter solenoid coils: reasonable agreement was found. Third, as a demonstration of the usefulness of such coils for mass-limited samples, multidimensional experiments were performed at 750 MHz on ~4.7 nmol (41 µg) of PF1061, a protein from *Pyrococcus furiosus*. Copyright © 2006 John Wiley & Sons, Ltd.

KEYWORDS: NMR; solenoidal coils; wire geometry; proximity effects; electromagnetic simulations; mass-limited samples; protein NMR

INTRODUCTION

The availability of high-field superconducting magnets, with corresponding Larmor frequencies approaching 1 GHz, has significantly enhanced the power of solution- and solid-state NMR to solve new problems in chemistry and biology. Considerable efforts and resources have also been devoted to the development of new NMR probe technology, which aims to reduce the required sample quantities or data acquisition time by optimizing the signal-to-noise (S/N). Particularly important in this regard have been recent developments in 'cryoprobe' technology.^{1–10} Another active area of recent research has been the improvements in NMR mass sensitivity via miniaturization of the

radio-frequency (r.f.) coil,^{11–19} which has shown several advantages over conventional large coils for applications with small amounts of sample such as high-throughput screening, natural product chemistry, mass-limited samples in structural biology, and combinatorial or small-scale chemical synthesis. Small r.f. coils have also opened up the area of multiple-coil or multiple-sample NMR for higher throughput^{20–25} or specialized applications in solvent suppression,²⁶ rapid data acquisition,²⁷ monitoring of reaction kinetics²⁸ or optimizing NMR detected capillary separations.²⁹ The intrinsic high sensitivity of the smaller coils can also be used to excite very large frequency bandwidths, allowing certain demanding pulse sequences to be run more efficiently.¹⁶

Previous quantitative studies on the geometry of small solenoid coils have focused on the optimization of the coil dimensions and winding parameters.^{30–32} However, the conductor geometry, which directly affects the coil loss, has not yet drawn much attention. This paper considers the effects of the choice between the two most commonly used wire geometries, round or rectangular, on the performance of small solenoidal coils for high-field NMR. First, a simple analytical model for current distribution in such coils is presented. The model was used to derive the optimum length-to-diameter ratio for coils constructed from wire with either rectangular or circular cross-sections. Second, a commercial full wave three-dimensional electromagnetic solver was used to check

[†]Dedicated to Professor David M. Grant of the University of Utah on the occasion of his 75th birthday, in recognition of the outstanding contributions he has made to the methodology of nuclear magnetic resonance and its application to a wide range of chemical topics over a long period of time.

*Correspondence to: Arthur S. Edison, Department of Biochemistry and Molecular Biology and McKnight Brain Institute, University of Florida, P.O. Box 100245, Gainesville, FL 32610-0245, USA.
E-mail: art@mbi.ufl.edu

Contract/grant sponsor: National Institutes of Health;

Contract/grant number: P41 RR16105.

Contract/grant sponsor: National Institute for Biomedical Imaging and Bioengineering; Contract/grant number: EB002343.

Contract/grant sponsor: SECSG structural genomics grant (PSI);

Contract/grant number: GM062407.

the validity of the simple analytical model, and also to compare simulated S/N estimations with experimental NMR spectra acquired with 2.5 mm and 1.0 mm-diameter solenoid coils. Third, using a 2 mm-long, 1 mm-diameter rectangular-wire solenoid, as a demonstration of the usefulness of such coils for mass-limited samples, multidimensional experiments were performed at 750 MHz on only ~ 4.7 nmol (41 μg) of PF1061, a protein from *Pyrococcus furiosus*.

Simple analytical approach

The development of a closed-form expression of the S/N in NMR spectroscopy following a $\pi/2$ excitation pulse has been discussed in many previous studies.³³ In small volume NMR, using solenoid coils of below ~ 2 mm in diameter, coil noise dominates that from the sample and the S/N of a point sample at the center of the coil can be expressed as:³³

$$S/N \propto \frac{B_1/i}{\sqrt{R_{\text{coil}}}} \quad (1)$$

In order to study the effects of wire geometry at a particular frequency, this expression can be written as:

$$S/N \propto \frac{B_1}{\sqrt{i^2 R_{\text{coil}}}} = \frac{B_1}{\sqrt{P_{\text{loss}}}} \quad (2)$$

where P_{loss} is the power loss in the coil. Since P_{loss} depends on the current distribution in the wire, it is reasonable to expect that the choice of round or rectangular wire may have a significant effect on S/N. Although P_{loss} can be calculated by means of full three-dimensional solutions to Maxwell's equations with complicated and expensive commercial packages, this method is not available to all research groups. Therefore, we first develop a very simple analytical model to provide a first-order approximation of the effects of conductor geometry and coil size.

Schematics of solenoid coils with round and rectangular wire are shown in Fig. 1(a) and (b). Wire dimensions, including the diameter of the round wire and the thickness and width of the rectangular wire, are at least 20 times the skin depth of copper at frequencies higher than 600 MHz. Therefore, it is reasonable to consider currents in the coil as surface currents. For perfect conductors of finite dimension, the magnetic fields normal to the surface vanish. This gives the boundary condition:³⁴

$$\vec{B} \cdot \vec{n} = 0 \quad (3)$$

In general, the current distribution on the cross-sectional area of the wire varies along the wire from the center to the two ends of the coil owing to finite coil length and associated wave phenomena,^{35,36} and there is no general analytical solution. To develop an analytical solution, we make two simplifying approximations. The first is that the current distribution in each turn is the same as in every other turn. We neglect the difference in the current distribution expected between turns at the end of the coil and in the center of the coil. This clearly becomes more accurate for

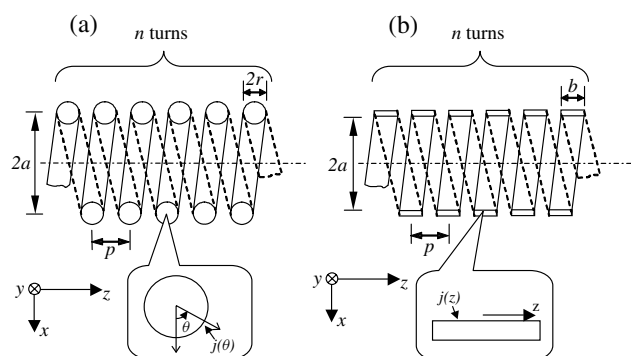


Figure 1. Schematic of solenoid coils wound with (a) round and (b) rectangular wire. The two inset figures are the expanded cross-sections of the conductor. The origin of the Cartesian coordinate system is at the center of the long axis of the coil. Parameters: a , coil radius; p , pitch; r , radius of round wire; b , width of rectangular wire; n , number of turns. As discussed in the text, since the current flows only on the inner surface of the rectangular conductor, the value of j depends only on z .

a larger number of turns and/or length-to-diameter ratio. The second approximation is that wave phenomena are negligible because the coil is well balanced and the conductor length for these small solenoids is much less than one wavelength.

The coordinate system used is shown in Fig. 1, and the two inset figures show the expanded cross-sectional areas of the wires at the centers of the two coils. The small pitch angle is neglected and thus there is no current component in the x - z plane. The surface current densities are written as $j(\theta)$ and $j(z)$ for round and rectangular wire, respectively. It should be noted that the small thickness of the rectangular wires is neglected and only the currents on lateral surfaces are considered, as in previous studies.^{34,37} Given this well-defined localization of the current, the analysis can then be treated as an electrostatic problem with a boundary condition given by Eqn (3) and the field on the surface of the center conductor can be evaluated by the Biot-Savart law:

$$\vec{B}(\vec{R}') = \frac{\mu_0}{4\pi} \iint \frac{j(s) ds \vec{d}\vec{l} \times (\vec{R}' - \vec{R})}{|\vec{R}' - \vec{R}|^3} \quad (4)$$

where s corresponds to either θ or z , depending on the conductor geometry (Fig. 1), $j(s)$ is the current density, $j(s) ds$ is a line current, \vec{l} is the solenoid curve that each line current follows on the conductor surface, \vec{R} is a space vector with three components equal to the coordinates of the point at which the solenoid curve \vec{l} intersects the cross section of the center conductor, and \vec{R}' is a space vector with three components equal to the coordinates of a point on the surface of the center conductor in a coil. Substitution of Eqn (4) into Eqn (3) yields

$$\iint \frac{j(s) ds \vec{d}\vec{l} \times (\vec{R}' - \vec{R}) \cdot \vec{n}(\vec{R}')}{|\vec{R}' - \vec{R}|^3} = 0 \quad (5)$$

In three-dimensional space, the solenoid curve \vec{l} can be represented by a set of standard parametric equations with

an angular parameter φ in the x - y plane. For round wire, the terms in Eqn (5) are

$$\begin{aligned}
 j(s)ds &= j(\theta)d\theta \\
 d\vec{l} &= \left[-(a+r(1+\cos\theta))\sin\varphi, \right. \\
 &\quad \left. (a+r(1+\cos\theta))\cos\varphi, \frac{p}{2\pi} \right] d\varphi \\
 \vec{R}' &= [a+r(1+\cos\theta'), 0, r\sin\theta'] \\
 \vec{R} &= \left[(a+r(1+\cos\theta))\cos\varphi, \right. \\
 &\quad \left. (a+r(1+\cos\theta))\sin\varphi, \frac{p}{2\pi}\varphi + r\sin\theta \right] \\
 \vec{n}(\vec{R}') &= [\cos\theta', 0, \sin\theta'] \\
 \theta &\in [0, 2\pi), \theta' \in [0, 2\pi), \varphi \in [-\pi, \pi] \quad (6)
 \end{aligned}$$

For rectangular wire the corresponding parameters are

$$\begin{aligned}
 j(s)ds &= j(z)dz \\
 d\vec{l} &= \left[-a\sin\varphi, a\cos\varphi, \frac{p}{2\pi} \right] d\varphi \\
 \vec{R}' &= [a, 0, z'] \\
 \vec{R} &= \left[a\cos\varphi, a\sin\varphi, \frac{p}{2\pi}\varphi + z \right] \\
 \vec{n}(\vec{R}') &= [-1, 0, 0] \\
 z &\in [-b/2, b/2], z' \in [-b/2, b/2], \varphi \in [-\pi, \pi] \quad (7)
 \end{aligned}$$

Assuming that unit current is fed into the solenoid coil, then,

$$\int_0^{2\pi} j(\theta)d\theta = 1 \quad (8)$$

and

$$\int_{-b/2}^{b/2} j(z)dz = 1 \quad (9)$$

Equations (5), (6) and (8) form a group of integral equations for solenoid coils constructed using round wire, and Eqns (5), (7) and (9) for coils using rectangular wire. The solutions to these equations give the current distributions on the surfaces of the two different conductors at the centers of the solenoid coils. The power loss in the coil has a strong dependence on the current distribution and can be written as³⁸

$$P_{\text{loss}} = K_{\text{round}} \int_0^{2\pi} j^2(\theta)d\theta \quad (10)$$

for round wire, and

$$P_{\text{loss}} = K_{\text{rectangular}} \int_{-b/2}^{b/2} j^2(z)dz \quad (11)$$

for rectangular wire, where K_{round} (Ohms) and $K_{\text{rectangular}}$ (Ohm-meters) are factors that account for all effects not related to the current distribution. A derivation of the values of K_{round} and $K_{\text{rectangular}}$ is given in the Appendix. The relative S/N can be expressed, as in a previous study,³⁴ in terms of a parameter q , given by

$$S/N \propto \sqrt{q} = \frac{B_1(0)}{\sqrt{P_{\text{loss}}}} \quad (12)$$

The software package Mathematica (Wolfram Research, Inc., Champaign, IL) was used to carry out the numerical calculations. The integral equations were solved numerically using the method described in a previous study.³⁹ The variables θ' , θ , z' , and z were discretized and the surface currents were modeled as a number of line currents within the solenoid curves. The integral equations were then converted into a group of linear equations which were solved by an inverse matrix operation. Using the resulting current densities, the quantity q was calculated.

The q values of a series of solenoid coils with different winding parameters are plotted vs length-to-diameter ratio in Fig. 2. It can be seen that there is an optimum length-to-diameter ratio of ~ 0.7 for a round-wire coil and ~ 1.0 for a rectangular-wire coil. Figure 2 also shows that the q values have a weak dependence on the number of turns. The results in Fig. 2(a) match well with two previous studies on Q optimization of solenoid coils,^{40,41} supporting the results of this simple model. It should be noted that the optimum length-to-diameter ratio for rectangular-wire coils is larger than that for round-wire coils.

Figure 3 shows the current distribution in two coils of round wire with significantly different length-to-diameter ratios. The results for the coil with a very small length-to-diameter ratio, 0.2 : 1, are consistent with previous analyses.³⁴ Most of the current flows on both the inner and outer sides of the wire because of the proximity effects between adjacent turns. However, the plot of the current distribution for the coil with a length-to-diameter ratio of 2 : 1 shows a different

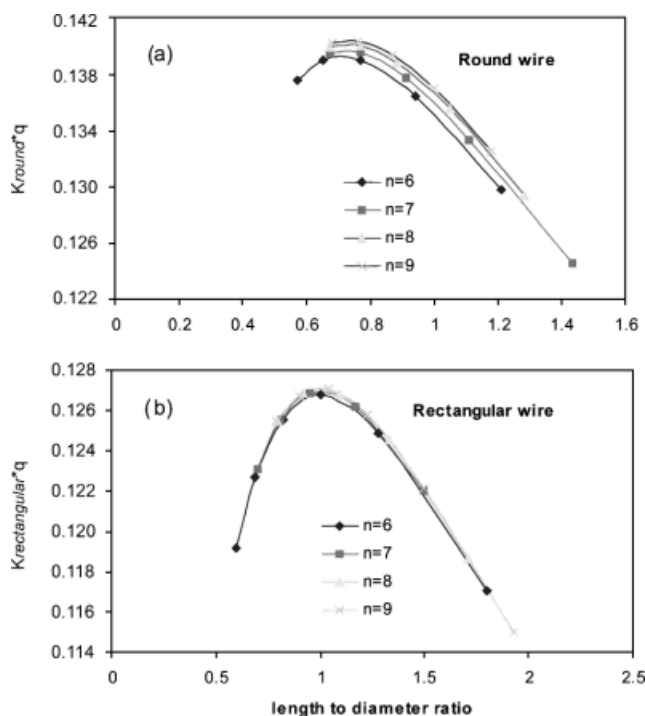


Figure 2. Plots of calculated q values vs length-to-diameter ratio and number of turns for small solenoid coils built from (a) round wires, and (b) rectangular wires. The coil diameter was nine times larger than the wire diameter for the round wire, and seven times larger than the longest dimension for the rectangular wire.

pattern – the current is concentrated on the inner side of the coil and the current uniformity within the wire is lower. Qualitatively, we can say that the current is attracted by the oppositely directed current on the other side of the coil. The attractive effect increases with the length-to-diameter ratio. As shown in Fig. 4, the attractive effect is even stronger in rectangular-wire coils than in round-wire coils.

Figure 5 shows the current distribution patterns in spaced and close-turn rectangular-wire solenoids. For the spaced turns, the current density difference between the center and edges of the conductor surface is as large as 50%. These edge effects can be suppressed by winding a solenoid coil with close turns, i.e. with near zero inter-turn distance. A current distribution plot in such a coil with the same length-to-diameter ratio is also shown in Fig. 5. The flat curve implies a relatively uniform current distribution across the wire. These results agree well with a previous study on current distribution in saddle coils built from rectangular wire.³⁴ This also suggests that a zero inter-turn distance in rectangular-wire coil should be used for the optimum S/N performance. With such a configuration, the solenoid coils built from rectangular wire have a more uniform current distribution than those constructed using round wires if the length-to-diameter ratio is large. For this reason, one expects

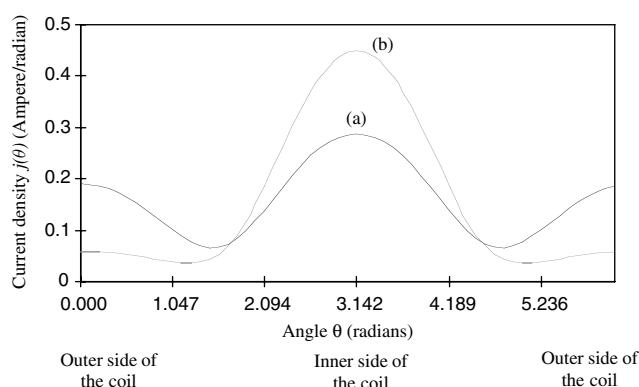


Figure 3. (a) Current distribution on conductors of a round-wire solenoid coil with winding parameters: coil length 2 mm, coil diameter 10 mm, wire diameter 0.24 mm, 6 turns. Currents are concentrated toward both the inner and outer sides of the coil. (b) Current distribution on conductors of a round-wire solenoid coil with winding parameters: coil length 2 mm, coil diameter 1 mm, wire diameter 0.24 mm, 6 turns. Currents are concentrated toward only the inner side of the coil.

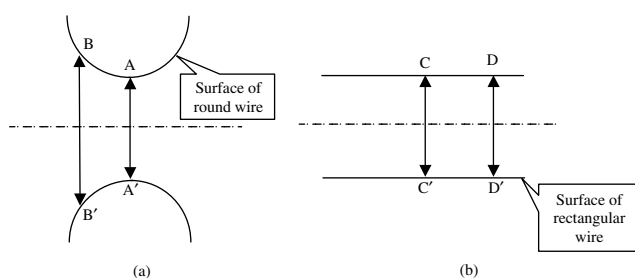


Figure 4. Spatial differences due to conductor geometry difference between (a) round wire and (b) rectangular wire in a solenoid coil.

a smaller power loss and hence a higher S/N in rectangular coils than in round-wire coils for a large value of this ratio.

Numerical 3D finite-element simulations

In order to assess the results from the simple analytical model presented above, we also used a commercial full wave 3D electromagnetic analysis tool (HFSS, Ansoft Corp., Pittsburgh, PA), based on the finite-element method. For purposes of the simulation, the coils were driven in a balanced mode by a current source in order to produce a current of amplitude 1 amp in the coil at the operating frequency of 750 MHz. A cylindrical shield of 5 mm in diameter and 4 mm in height defined the boundary of the simulation. The current density on the inner surface of the rectangular coils was found to be almost five-times higher than on the outer surface, this justifies the assumption used in the analytical model that all current in the close-wound rectangular coil flows on the inner surface of the wire. For the 1 amp drive current, B_1 and P_{loss} were evaluated separately. The power dissipation was calculated by evaluating the Poynting vector (the normal component of the $E \times H^*$, where the quantities E and H are the electric and magnetic field intensities) over the entire surface of the wire. Sample loss was neglected. Simulations were performed for four coils, the physical design parameters of which are shown in Table 1. The relative S/N ratios of coils constructed using round wires and rectangular wires are shown in Table 2. In each case, the B_1 fields produced by coils 1 and 2, and coils 3 and 4 were very similar, with the S/N differences arising primarily as a result in the differences in power dissipation, as expected.

Experimental signal-to-noise measurements

Solenoid coils with diameters of 1.0 mm and 2.5 mm were fabricated using copper wires of different geometries and dimensions as shown in Table 1. The wires were wound on a small capillary, which was used to hold the samples.

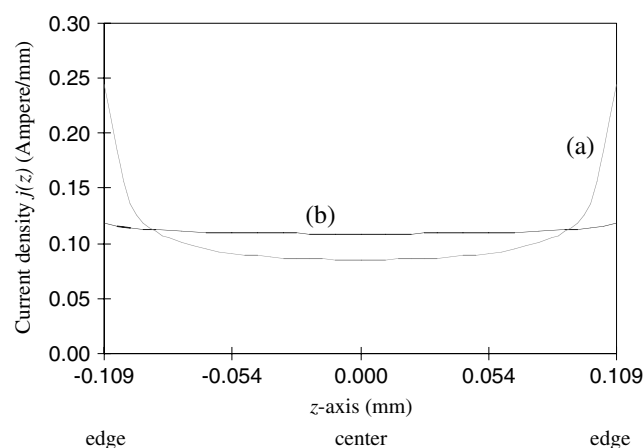


Figure 5. (a) Current distribution pattern of a spaced-turn solenoid coil of rectangular wires with winding parameters: $2a = 1$ mm, $b = 0.23$ mm, $p = 0.36$ mm, $n = 6$. Severe current crowding occurs at the two edges of the wire. (b) Current distribution pattern of a close-turn solenoid coil of rectangular wires with winding parameters: $2a = 1$ mm, $b = 0.23$ mm, $p = 0.23$ mm, $n = 6$. Currents are relatively uniform across the wire.

Table 1. Winding parameters of the four solenoid coils used for S/N comparisons

Solenoid coil ID#	Coil diameter (mm)	Turn number	Coil length (mm)	Wire geometry	Wire dimension (mm)
1	2.5	4	1.7	Round	0.287
2	2.5	4	1.7	Rectangular	0.05 × 0.38
3	1.0	8	2.0	Round	0.15
4	1.0	8	2.0	Rectangular	0.05 × 0.23

Table 2. Relative S/N comparison of the four solenoid coils using the full three-dimensional finite-element simulation and data from experiment

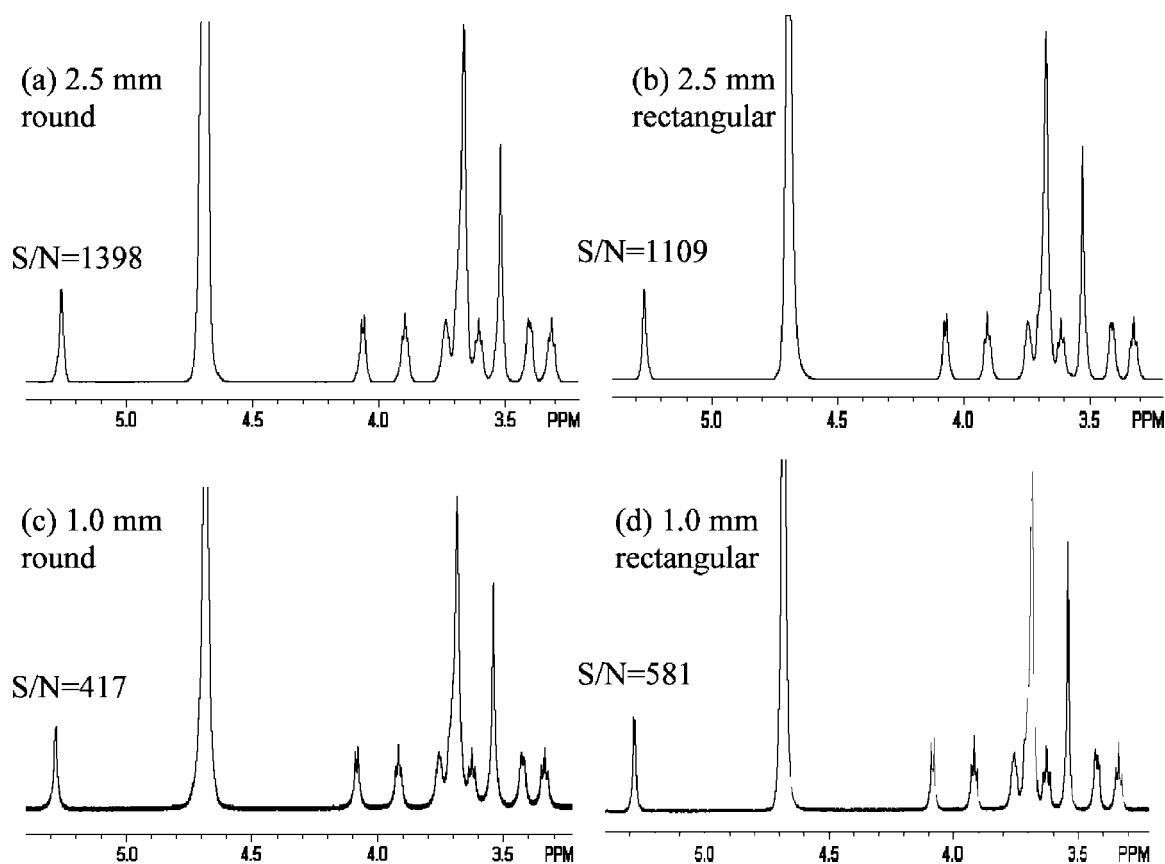
	Finite-element	Experiments
Coil #2/Coil #1	0.9	0.79
Coil #4/Coil #3	1.47	1.39

Table 3 shows values of coil inductance and loaded (Q_L) and unloaded (Q_U) Q values. Standard 1D ^1H NMR experiments were performed to measure the experimental S/N using different coils on a Bruker Avance 750 MHz spectrometer. Susceptibility-matching fluid (FC-43, 3M Corp., St Paul, MN) was used to improve the B_0 homogeneity, as described previously.¹⁴ The sample used for S/N measurements of

Table 3. Measurement of reference parameters of the four solenoid coils in bench and experiment test

Solenoid coil ID #	Inductance (nH)	Q_U/Q_L values	90° pulse length ($\mu\text{s}@0.4\text{ W}$)	Half-height linewidth of water peak (Hz)
1	47	113/78	8.9	9.0
2	49	105/75	9.5	8.0
3	65	103/81	3.6	6.0
4	59	93/78	3.8	5.2

the coil was 100 mM sucrose in 100% D_2O , and shimming was performed on the residual HOD peak. The 90° pulse calibration results in Table 3 show that the B_1 fields produced by coils built from round wire (coil 1 and 3) are slightly stronger than those from rectangular wires (coil 2 and 4). This is a reasonable result because the current path of a spaced solenoid coil built from round wires is closer to the center point of the coil in the long-axis direction than that of a nonspaced solenoid coil built from rectangular wires. The lower B_1 field in coil 4 than that in coil 3 further proves that the higher S/N in coils built from rectangular wires primarily arises from lower power dissipation, as expected. Figure 6 shows NMR spectra of 100 mM sucrose acquired using the different coils. The linewidths are reported in Table 3. It should be noted that these linewidths are considerably

**Figure 6.** Sucrose spectra acquired using (a) coil #1, (b) coil #2, (c) coil #3, and (d) coil #4 in Table 1. The S/N was measured on the anomeric peak of sucrose at ~5.4 ppm. Data acquisition parameters: acquisition time 1.4 s, spectral width 3754 Hz, number of complex data points 5254, number of scans 8, line-broadening of 0.7 Hz was applied.

broader than are typical values (<1 Hz) obtained using small solenoidal coils. This is attributed mainly to the system having been designed primarily for microimaging, and therefore being equipped only with very weak, lower order, large diameter shims. The S/N was measured on the doublet of the anomeric sucrose peak at 5.3 ppm. The difference in linewidths was accounted for by integrating over the doublet. The measurements show that the S/N for the 2.5 mm round-wire coil is higher than that for the rectangular-wire coil of the same diameter, but that the situation is reversed for the 1-mm diameter coils. The relative S/N ratios are also shown in Table 2 and agree well with the simulation results.

Acquisition of heteronuclear protein NMR spectra using a 1-mm diameter rectangular-wire coil

The rectangular-wire 2 mm-long 1.0 mm-diameter coil was used to acquire data from a stable protein, PF1061, an 8.7 kDa protein⁴² from *P. furiosus*. The plasmid was provided by the Southeast collaborative for structural genomics (SECSG), and the protein was expressed in M9 minimal media supplemented with ^{15}N -ammonium chloride and ^{13}C -glucose and purified according to protocols developed in the SECSG.⁴² The protein concentration was 4 mM in 90% $\text{H}_2\text{O}/10\%$ D_2O containing 100 mM potassium phosphate (pH 5.5) and 100 mM KCl. DSS (2,2-dimethyl-2-silapentane-5-sulfonic acid)

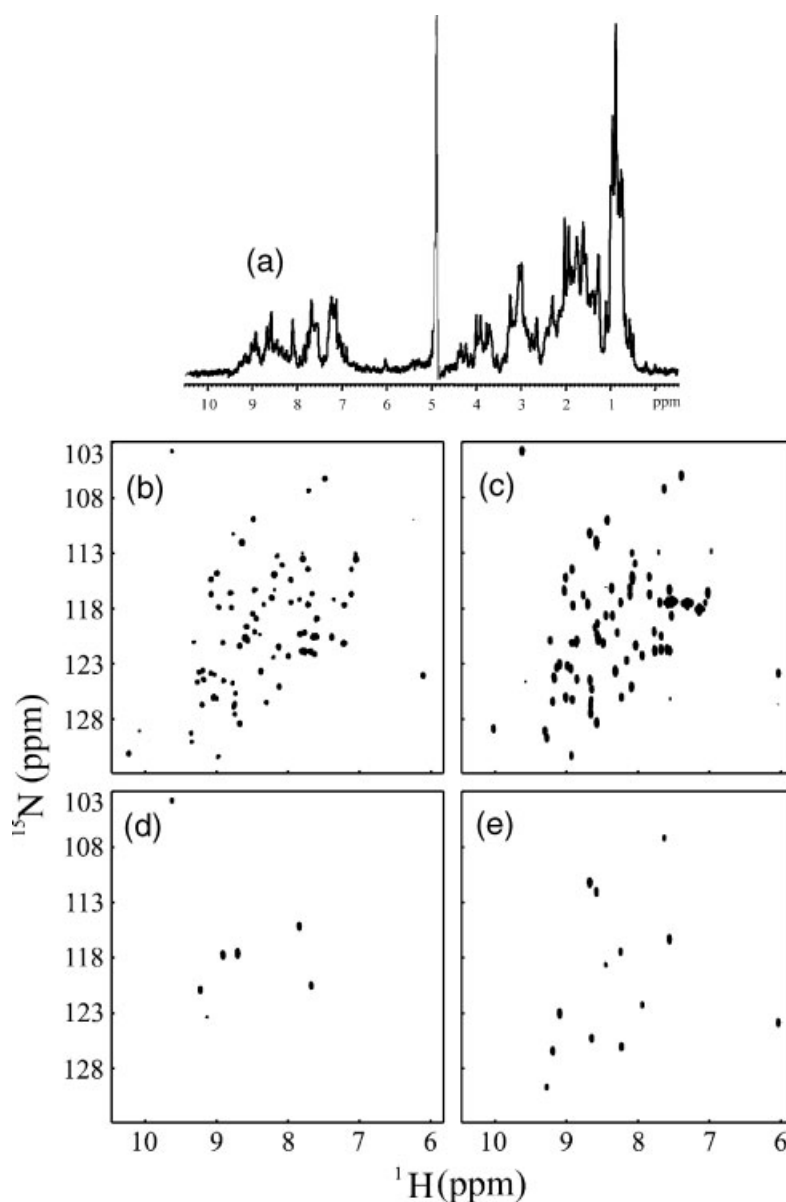


Figure 7. NMR data on 4 mM PF1061 protein in a 1.2 μl active volume of a 1-mm rectangular-wire coil. (a) 1D NMR spectrum collected with eight scans and WATERGATE water suppression. The 2D ^{15}N -HSQC spectrum (b) is compared to the projection of the $^{13}\text{C}'$ dimension of a 3D HNCO spectrum (c). Slices of the HNCO spectrum at 176.3 ppm (d) and 175.8 ppm (e) are shown below. Two-dimensional ^{15}N -HSQC data were collected in about 45 min using eight scans and 4096 and 256 complex points in t_2 and t_1 , respectively. Three-dimensional HNCO data were collected in about 20 h using eight scans and 2048, 120, and 64 complex points for ^1H , ^{13}C , and ^{15}N , respectively. For all datasets, the ^1H carrier frequency was placed on water, and spectral widths for the HNCO experiment were 13 ppm for ^1H , 33.7 ppm for ^{15}N , and 20.4 ppm for ^{13}C . Data were processed using NMRPipe⁴⁴ and visualized using NMRView.⁴⁵

was added as an internal ^1H and indirect ^{15}N and ^{13}C reference. The probe body built for this study was used in a 17.6 T/89 mm wide-bore magnet, and three-axis gradients were placed on the outside of the probe. The active sample volume was 1.2 μl , and contained only about 4.7 nmol ($\sim 41 \mu\text{g}$) of protein in the active volume of the probe. This is approximately 3-times less sample than previously reported using a commercial microcoil probe for protein triple resonance studies.¹⁶ The 90° pulse lengths were: ^1H 4.5 μs @ 0.4 W, ^{15}N 9.0 μs @ 75 W and ^{13}C 4.7 μs @ 18 W. Figure 7 shows, first, a 1D ^1H spectrum collected with eight scans using WATERGATE.⁴³ In order to test the performance of the coil in standard protein NMR experiments, we also collected 2D ^{15}N -HSQC and 3D HNCO triple resonance datasets (Fig. 7). All the multidimensional protein datasets have good S/N, showing that useful data can be obtained on very small amounts of sample using small, optimized r.f. coils.

DISCUSSION

This paper has presented results, from both a simple analytical model and full three-dimensional finite-element simulations, of the current distribution in solenoid coils with different length-to-diameter ratios and conductor geometries. General findings can be summarized as follows: (i) relatively high currents are concentrated toward the inner side of a solenoid coil with a large length-to-diameter ratio and this effect is more pronounced in coils made from rectangular wire than those from round wire; (ii) the current uniformity in the turns of a solenoidal coil constructed from rectangular wire suggests that a zero inter-turn space is optimum for small coils of this geometry, although further experimental verification needs to be performed; (iii) if the length-to-diameter ratio of the coils is large, the coil loss in a close-turn solenoid coil constructed of rectangular wire is lower than that in a spaced-turn coil of round wire. We attribute this to the exceptionally uniform current distribution in a close-turn solenoid coil wound using rectangular wire, as compared to the nonuniform current distribution in the round-wire coil.

Finally, it was demonstrated that a 1-mm diameter solenoid coil was capable of acquiring high quality multiple-resonance data on as little as $\sim 40 \mu\text{g}$ (4.7 nmol) protein samples. This technology, therefore, has great potential promise in sample savings in applications such as protein-based molecular library screening.

Acknowledgements

NMR data were collected in the AMRIS facility of the McKnight Brain Institute of the University of Florida. We thank James Rocca in the MBI AMRIS facility for help with NMR experiments. The plasmid for the protein used in this study was kindly provided by the Mike Adams lab and the SECSG structural genomics grant (PSI) (GM062407), and we thank James Prestegard of the University of Georgia and members of his lab for protocols for expression and purification of the protein. The contribution of William Brey and Saikat Saha was supported by the National Science Foundation Cooperative Agreement (DMR 00884173) and the State of Florida through the NHMFL. This paper is dedicated to Professor David Grant who taught ASE general chemistry, provided him with undergraduate research opportunities, and demonstrated that science is an outstanding career.

APPENDIX

This Appendix contains derivations of the constants K_{round} and $K_{\text{rectangular}}$. As in the analytical model, these derivations make the simplifying assumption of a uniform effective skin depth within the conductor along its length.

Derivation of K_{round}

Equation (10) states that, for a solenoid of round wire, neglecting the end effects:

$$P_{\text{loss}} = K_{\text{round}} \int_0^{2\pi} j^2(\theta) d\theta \quad (13)$$

The constant K_{round} comprises all of the effects that are not part of the angular current distribution. One can determine the value of P_{loss} for a coil for which the current does not depend on θ and solve for K_{round} . For such a coil, if I is the total current, then,

$$\int_0^{2\pi} j(\theta) d\theta = I \quad (14)$$

The value of $j(\theta)$ is constrained to be a constant j_{is} (free space), in which case $j_{\text{is}} = I/2\pi$. For this simple case, one can write the power loss in terms of the skin depth surface resistance R_{SR} as

$$P_{\text{loss}} = I^2 R_{\text{SR}} \quad (15)$$

The surface resistance is just a simple function of skin depth δ , the wire radius r , the wire length L , and the bulk resistivity ρ :

$$R_{\text{SR}} = \frac{\rho L}{2\pi r \delta} \quad (16)$$

Now, setting Eqns (13) and (16) equal to one another, and solving for K_{round} :

$$K_{\text{round}} = \frac{\rho L}{r \delta} \quad (17)$$

Since ρ has units of $\Omega\text{-m}$, K_{round} has units of Ω .

Derivation of $K_{\text{rectangular}}$

Starting from Eqn (11) for wire of width b :

$$P_{\text{loss}} = K_{\text{rect}} \int_{-b/2}^{b/2} j^2(z) dz \quad (18)$$

and applying the normalization condition

$$\int_{-b/2}^{b/2} j(z) dz = I \quad (19)$$

A uniform surface current distribution is assumed across the inner side of the wire: $j(z) = j_c$, and then the condition $j_c = I/b$ can be derived. The surface resistance of the wire is given by

$$R_{\text{SR}} = \frac{\rho L}{b \delta} \quad (20)$$

Setting Eqns (18) and (20) equal to one another and solving for K_{rect} :

$$K_{\text{rect}} = \frac{\rho L}{\delta} \quad (21)$$

Since ρ has units of $\Omega\text{-m}$, K_{rect} also has units of $\Omega\text{-m}$.

REFERENCES

1. Wong WH, Withers RS, Nast R, Kotsubo VY, Johansson ME, Hill HDW, Fuks LF, Kelin KA, Cole B, Brey WW, Barfknecht A, Anderson WA. *Adv. Cryog. Eng.* 1996; **42**: 953.
2. Logan TM, Murali N, Wang GS, Jolivet C. *Magn. Reson. Chem.* 1999; **37**: 762.
3. Crouch RC, Llanos W, Mehr KG, Hadden CE, Russell DJ, Martin GE. *Magn. Reson. Chem.* 2001; **39**: 555.
4. Russell DJ, Hadden CE, Martin CE, Gibson AA, Zens AP, Carolan JL. *J. Nat. Prod.* 2000; **63**: 1047.
5. Griffin JL, Keun H, Richter C, Moskau D, Rae C, Nicholson JK. *Neurochem. Int.* 2003; **42**: 93.
6. Keun HC, Beckonert O, Griffin JL, Richter C, Moskau D, Lindon JC, Nicholson JK. *Anal. Chem.* 2002; **74**: 4588.
7. Hill HDW. *IEEE Trans. App. Supercon.* 1997; **77**: 3750.
8. Flynn PF, Mattiello DL, Hill HDW, Wand AJ. *J. Am. Chem. Soc.* 2000; **122**: 4823.
9. Horiuchi T, Takahashi M, Kikuchi J, Yokoyama S, Maeda H. *J. Magn. Reson.* 2005; **174**: 34.
10. Kovacs H, Moskau D, Spraul M. *Prog. NMR Spectrosc.* 2005; **46**: 131.
11. Webb AG. *Prog. NMR Spectrosc.* 1997; **31**: 1.
12. Lacey ME, Subramanian R, Olson DL, Webb AG, Sweedler JV. *Chem. Rev.* 1999; **99**: 3133.
13. Li Y, Logan TM, Edison AS, Webb A. *J. Magn. Reson.* 2003; **164**: 128.
14. Olson DL, Peck TL, Webb AG, Magin RL, Sweedler JV. *Science* 1995; **270**: 1967.
15. Wu NA, Peck TL, Webb AG, Magin RL, Sweedler JV. *Anal. Chem.* 1994; **66**: 3849.
16. Peti W, Norcross J, Eldridge G, O'Neil-Johnson M. *J. Am. Chem. Soc.* 2004; **126**: 5873.
17. Gronquist M, Meinwald J, Eisner T, Schroeder FC. *J. Am. Chem. Soc.* 2005; **127**: 10 810.
18. Wolters AM, Jayawickrama DA, Sweedler JV. *Curr. Opin. Chem. Biol.* 2002; **6**: 711.
19. Webb AG. *J. Pharm. Biomed. Anal.* 2005; **38**: 892.
20. Hou T, MacNamara E, Raftery D. *Anal. Chim. Acta* 1999; **400**: 297.
21. MacNamara E, Hou T, Fisher G, Williams S, Raftery D. *Anal. Chim. Acta* 1999; **397**: 9.
22. Macnaughtan MA, Hou T, Xu J, Raftery D. *Anal. Chem.* 2003; **75**: 5116.
23. Raftery D. *Anal. Bioanal. Chem.* 2004; **378**: 1403.
24. Li Y, Wolters AM, Malawey PV, Sweedler JV, Webb AG. *Anal. Chem.* 1999; **71**: 4815.
25. Wang H, Ciobanu L, Edison AS, Webb AG. *J. Magn. Reson.* 2004; **170**: 206.
26. Macnaughtan MA, Smith AP, Goldsbrough PB, Santini RE, Raftery D. *Anal. Bioanal. Chem.* 2004; **378**: 1520.
27. Wang H, Ciobanu L, Webb A. *J. Magn. Reson.* 2005; **173**: 134.
28. Ciobanu L, Jayawickrama DA, Zhang XZ, Webb AG, Sweedler JV. *Angew. Chem., Int. Ed. Engl.* 2003; **42**: 4669.
29. Wolters AM, Jayawickrama DA, Webb AG, Sweedler JW. *Anal. Chem.* 2002; **74**: 5550.
30. Peck TL, Magin RL, Lauterbur PC. *J. Magn. Reson., Ser. B* 1995; **108**: 114.
31. Minard KR, Wind RA. *Conc. Magn. Reson.* 2001; **13**: 190.
32. Minard KR, Wind RA. *Conc. Magn. Reson.* 2001; **13**: 128.
33. Hoult DI, Richards RE. *J. Magn. Reson.* 1976; **24**: 71.
34. Carlson JW. *Magn. Reson. Med.* 1986; **3**: 778.
35. Ryff PF. *IEEE Trans. Industrial App.* 1972; **IA-8**: 485.
36. Engelke F. *Conc. Magn. Reson.* 2002; **15**: 129.
37. Guo J, Kaifez D, Glisson AW. *Electron. Lett.* 1997; **33**: 966.
38. Butterworth S. *Wireless Engineer* 1926; **3**: 309.
39. Labiche A, Kan S, Leroy-Willig A, Wary C. *Rev. Sci. Instrum.* 1999; **70**: 2113.
40. Kan S, Gonord P. *Magn. Reson. Med.* 1992; **23**: 372.
41. Wiseman RW, Moerland TS, Kushmerick MJ. *NMR Biomed.* 1993; **6**: 153.
42. Valafar H, Mayer KL, Bougault CM, LeBlond PD, Jenney FE Jr, Brereton PS, Adams MW, Prestegard JH. *J. Struct. Funct. Genomics* 2004; **5**: 241.
43. Piotta M, Saudek V, Sklenar V. *J. Biomol. NMR* 1992; **2**: 661.
44. Delaglio F, Grzesiek S, Vuister GW, Zhu G, Pfeifer J, Bax A. *J. Biomol. NMR* 1995; **6**: 277.
45. Johnson BA, Blevins RA. *J. Biomol. NMR* 1994; **4**: 603.